Uppsala University

Department of Physics and Astronomy

Project in Physics and Astronomy

1FA195

Time-optimal holonomic quantum computation

Author: Gabriel Oliveira Alves
Supervisor: Erik Sjöqvist

April 12, 2022

Abstract

A three-level system can be used in a Λ-type configuration in order to construct a universal set of non-adiabatic quantum gates through the use of non-Abelian non-adiabatic geometrical phases. Such construction allows for high-speed operation times which diminish the effects of decoherence. This might be, however, accompanied by a breakdown of the validity of the rotating wave approximation (RWA) due to the comparable timescale between the counter-rotating terms and the pulse length, which greatly affects the dynamics. Here we investigate the trade-off between dissipative effects and the RWA validity, obtaining the optimal regime for the operation of the holonomic quantum gates.

Acknowledgements

I would like to start by thanking Erik Sjöqvist for his guidance and for his patience during the development of this project. His willingness to discuss physics and to introduce me to this field have been invaluable.

I would also like to thank Carlos Moysés Graça Araujo for coordinating this exchange program and also for his help regarding my stay in Uppsala. Without his aid this project certainly would not be possible.

I am also thankful to all the friends I made during my stay in Uppsala: Nader, Umer, Paula, Sorana, Arsalan, Felix, Artur, Shila, Ingrid, Mostafa, Marco, Mo, Bilal, Ali, Umair and Zeeshan.

Finally, I also acknowledge the staff in the Uppsala university, the staff in University of São Paulo and the financial support given by the European Commission through the Swedish Council for Higher Education in the framework of Erasmus+ KA107

Contents

1 Introduction

The advent of quantum mechanics in the past century has brought a plethora of different technologies. Quantum computing, for instance, has shown several promising applications throughout the years. A few seminal works, such as the ones by Deutsch [1] and Shor [2], and even protocols for quantum-key distribution [3], have established a new ground for quantum technologies, showcasing how quantum mechanics can be used to optimize tasks in computation and information processing.

However, quantum computing (QC) naturally requires a suitable platform to be performed on. An appropriate platform for QC has several desirable properties, such as scalability [4], robustness against errors [5–7], long decoherence times [8, 9] and universality [10]. Thus the search for such a platform is, in itself, an extensive area of research, one which has seen considerable progress over the last decades. Proposals range from trapped ions [11] to topological systems [12].

Among them, one promising alternative is holonomic quantum computing, which emerged at the end of the nineties [13, 14]. This approach is based on the use of geometrical phases for quantum computing due to certain advantages such as its robustness against certain types of errors and noise. Even within the field of holonomic quantum computing, several different implementations and protocols have been proposed. For a review on these topics, see e.g. [15].

In this work we try to examine some of these different implementations, focusing our attention on a non-adiabatic scheme for quantum computing based on Λ-type systems, proposed in [16]. This framework has seen a couple of generalizations and alternative constructions in the last few years, together with concrete experimental implementations. Our main focus here is to study this implementation outside the regime of validity of the rotating wave approximation (RWA).

In Sec. 1 we review basic concepts about geometrical phases, with special focus on non-Abelian non-adiabatic phases. In Sec. 2 we review the proposal for non-adiabatic quantum computing using Λ-type systems and we introduce some of our results for the non-RWA case. In Sec. 3 we review the formalism for open quantum system using Lindblad master equations and finally, in Sec. 4, we discuss our main results. Conclusions and future outlooks can be found in Sec. 5.

1.1 The geometrical phase

In his seminal work, Berry [17] showed how geometrical phases arise in quantum mechanical systems and its physical consequences. The results by Wilczek and Zee [18] made further advancements, making a generalization for the degenerate case and showing how a non-Abelian structure can emerge. A few years later, important

contributions by Aharonov and Anandan [19, 20] came out, further generalizing the non-Abelian geometric phase from Wilczek and Zee to the non-adiabatic case. Here we briefly review the results by Berry, Aharonov and Anandan.

1.2 Berry's Phase

The simplest case we will consider is the Berry phase, a geometrical phase which can emerge when the system evolves adiabatically; which means that the Hamiltonian is varied very slowly. By doing so, the evolution in the Hilbert space follows the instantaneous eigenstates of the Hamiltonian.

More concretely, consider a Hamiltonian $H(\mathbf{R}(t))$ which depends on a vector of parameters $\mathbf{R}(t) = (R_1, R_2, ...)$. Let us also consider initially a non-degenerate case. The eigenstates $|n(\mathbf{R}(t))\rangle$ of this Hamiltonian will naturally depend on the parameters:

$$H(\mathbf{R}(t))\,|n(\mathbf{R}(t))\rangle = \epsilon_n(\mathbf{R}(t))\,|n(\mathbf{R}(t))\rangle\,. \tag{1.2.1}$$

The adiabatic theorem states that a state which is initially the n-th eigenstate of H,

$$|\psi_n(0)\rangle = |n(\mathbf{R}(0))\rangle \tag{1.2.2}$$

will evolve into the instantaneous eigenstate of H at a later time t, that is

$$|\psi_n(t)\rangle = c_n(t)\,|n(\mathbf{R}(t))\rangle\,, \tag{1.2.3}$$

given that the evolution is sufficiently slow. In this sense, the time scale is defined by the inverse of the energy gap between the energy of the n-th state and the neighboring states; the smaller the gap the slower the process should be. This establishes a mapping between the path in the parameter space and a path in the Hilbert space of the wave functions. The coefficient in Eq. (1.2.3) can be written as:

$$c_n(t) = e^{i\gamma_n(t)} \exp\left[-i\int_0^t dt' \epsilon_n(t')\right]. \tag{1.2.4}$$

The second factor in the equation above is called *the dynamical phase* [21]. Our objective of interest, however, is precisely the phase γ_n. By plugging the equation above and Eq. (1.2.3) into the the Schrödinger equation (SE) $i\hbar\frac{d}{dt}\,|\psi_n\rangle = H(\mathbf{R}(t))\,|\psi_n\rangle$, we get, after taking the inner product with $\langle\psi(t)|$ [22]:

$$\gamma_n(t) = i\int_0^t dt'\,\langle n(\mathbf{R}(t'))|\,\frac{d}{dt'}\,|n(\mathbf{R}(t'))\rangle\,. \tag{1.2.5}$$

The geometrical aspect of the above equation becomes evident if we make one

further modification. By using the chain rule to write

$$\frac{d}{dt}\left|n(\mathbf{R}(t))\right\rangle = \nabla_{\mathbf{R}}\left|n(\mathbf{R}(t))\right\rangle \cdot \frac{d\mathbf{R}}{dt}, \tag{1.2.6}$$

we may recast Eq.(1.2.5) as

$$\gamma_n(t) = \int_C \mathcal{A}^n(\mathbf{R}) \cdot d\mathbf{R}, \tag{1.2.7}$$

where

$$\mathcal{A}^n(\mathbf{R}) = i\left\langle n(\mathbf{R})\right| \nabla_{\mathbf{R}}\left|n(\mathbf{R})\right\rangle \tag{1.2.8}$$

is called the *Berry connection*. This result is remarkable because it reveals a novel interpretation of γ_n. This phase is not an explicit function of the time, but rather, it depends only on the path C of $\mathbf{R}$ in the parameter space, irrespective of the dynamical details of the evolution. Hence, this phase is regarded as a geometrical phase.

One important detail, however, is that this phase typically behaves like a gauge. So, if we change the eigenstate by a phase $\delta(\mathbf{R})$, a change in the Berry connection (1.2.8) also incurs:

$$\left|n(\mathbf{R})\right\rangle \to e^{\delta(\mathbf{R})}\left|n(\mathbf{R})\right\rangle \implies \mathcal{A}^{\mathbf{n}}(\mathbf{R}) \to \mathcal{A}^{\mathbf{n}}(\mathbf{R}) - \nabla_{\mathbf{R}}\delta(\mathbf{R}). \tag{1.2.9}$$

This results in a phase change which depends on the endpoints of this gauge, in other words:

$$\gamma_n \to \gamma_n + \delta(\mathbf{R}(0)) - \delta(\mathbf{R}(t)). \tag{1.2.10}$$

A important observation which can be made here [17] is that *cyclic* adiabatic processes in the *parameter* space, i.e. evaluations for which $\mathbf{R}(t_{end}) = \mathbf{R}(0)$ dispel the gauge-dependence in the geometrical phase, unambiguously defining a Berry connection for this cyclic evolution:

$$\gamma_n(t) = \oint \mathcal{A}^{\mathbf{n}}(\mathbf{R}) \cdot \mathbf{dR}. \tag{1.2.11}$$

The geometrical interpretations of this result are even more far reaching. For instance, one may notice that the Berry connection, due to its gauge properties, is strongly analogous to the vector potential of a magnetic field. It is also possible to define a Berry curvature, which is tensor constructed from the Berry connection. This allows us to use Stokes' theorem to express the geometrical phase (1.2.11) in terms of the area enclosed by the loop in the parameter space [22].

1.3 Non-adiabatic non-Abelian geometrical phase

A natural question which arises from Berry's framework is whether a similar result holds for a non-adiabatic evolution. Built upon Berry's work and also on the Wilczek-Zee phase, which is a previous generalization of Berry's phase for the degenerate case, it was shown that it is possible to obtain a non-adiabatic non-Abelian geometrical phase [19, 20] under certain conditions. This result will be vital for the construction of quantum gates later on, as we shall see.

Our objective in this section is to follow the approaches in [19] and [20] to obtain a closed form expression for the desired non-adiabatic non-Abelian geometrical phases. We begin by investigating the non-adiabatic (but Abelian) phase studied in [19]. This approach is slightly more general in the sense that we consider the Hilbert space $\mathcal{H}$ (with $\dim \mathcal{H} = n$) and its projective space of rays, i.e. the set of rays $\mathcal{P}$ (with $\dim \mathcal{P} = n - 1$) defined by the projection map $\Pi : \mathcal{H} \to \mathcal{P}$ with $\Pi(|\psi\rangle) = \{|\psi'\rangle : |\psi'\rangle = c\,|\psi\rangle\,, \quad \text{s.t. } c \in \mathbb{C}\}$. In short, what Aharonov and Anandan did was to show that it is possible to compute a geometrical phase for *all* cyclic evolutions. This framework, and later on the generalization for the non-Abelian case [20], thus contain other well known special cases, such as the Berry phase, periodic dynamics (such as the procession of a particle in a constant magnetic field) and so on.

Trying to analyze Berry's phase and the trajectory of the state in the parameter space for a system with a degenerate subspace is one of the examples which illustrate why this new approach can be seen as more general. Curves in the parameter space, presented in the previous section, can show a certain redundancy in this case, since for a degenerate part of the eigenspace the curve in the projective Hilbert space will simply be a point in the parameter space [20]. This dynamics nevertheless still describes a proper loop in the space of rays $\mathcal{P}$, with an associated non-trivial geometrical phase.

More concretely, let us start by considering a normalized state $|\psi(t)\rangle \in \mathcal{H}$ which evolves according to the Schrödinger equation

$$H(t)\,|\psi(t)\rangle = i\hbar \frac{d}{dt}\,|\psi(t)\rangle \tag{1.3.1}$$

up to a time τ, which satisfies $|\psi(\tau)\rangle = e^{i\phi}\,|\psi(0)\rangle$. This evolution defines an arbitrary curve $\hat{C}$ in the Hilbert space $\mathcal{H}$. In the ray space $\mathcal{P}$ however this represents a closed loop $C = \Pi(\hat{C})$.

Now, define a state $|\tilde{\psi}(t)\rangle = e^{-if(t)}\,|\psi(t)\rangle$ with $f(\tau) - f(0) = \phi$. The evolution will be cyclic in the ray space since $|\tilde{\psi}(\tau)\rangle = |\tilde{\psi}(0)\rangle$ and the SE yields:

$$\frac{df}{dt} = \langle\tilde{\psi}(t)|\, i\frac{d}{dt}\,|\tilde{\psi}(t)\rangle - \frac{1}{\hbar}\,\langle\psi(t)|\, H\,|\psi(t)\rangle\,. \tag{1.3.2}$$

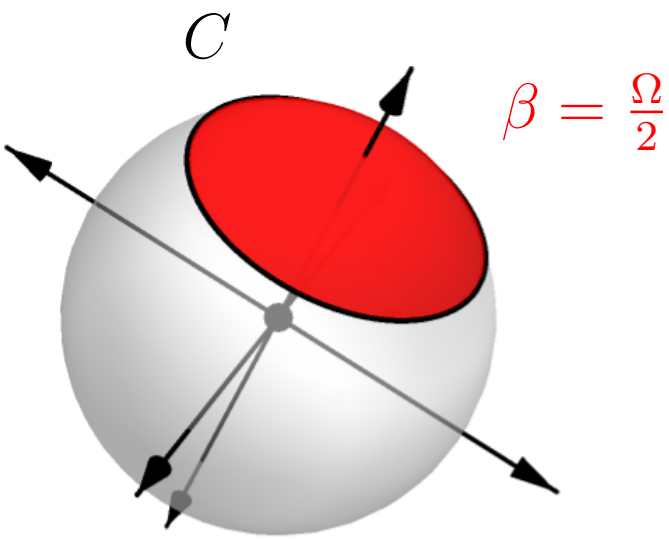

Figure 1: Loop C on the Bloch sphere for the periodic evolution of a qubit under a constant magnetic field. The geometrical phase acquired by the qubit corresponds to half the value of the solid angle associated with the loop.

By defining

$$\beta \equiv \phi + \frac{1}{\hbar}\int_0^\tau \frac{1}{\hbar}\,\langle\psi(t)|\,H\,|\psi(t)\rangle\,dt \tag{1.3.3}$$

we can integrate Eq. (1.3.2) to obtain:

$$\beta = \int_0^\tau \langle\tilde{\psi}(t)|\,i\frac{d}{dt}\,|\tilde{\psi}(t)\rangle\,dt. \tag{1.3.4}$$

This identity shows that the phase β is purely geometrical and depends only on the curve C in $\mathcal{P}$: β is independent of both ϕ and H. Moreover, $H(t)$ can even be chosen in an alternative definition so that the dynamical term in (1.3.3) vanishes. Note how no approximations were made here and the expression for the phase β is exactly valid: the evolution needs not to be slow neither the state $|\psi(t)\rangle$ needs to be an eigenstate of $H(t)$. As a side note, we can also check that by taking $|\tilde{\psi}(t)\rangle \approx |n(t)\rangle$ we recover Berry's result (1.2.5), where $|n(t)\rangle$ corresponds to an instantaneous eigenstate of $H(t)$.

If one is interested in measuring the geometrical phase (1.3.3), a few strategies are possible. One may tune H in such a way that the second term in Eq. (1.3.3) is zero, i.e. effectively eliminating the dynamical contribution from the phase, such that ϕ becomes purely geometrical. Another possible strategy is to evolve two different states such that their dynamical part is the same, so the geometrical phase (difference) can be measured through $\phi_1 - \phi_2 = \beta_1 - \beta_2$.

An interesting example is the periodic evolution of a qubit subject to a constant magnetic field in the z-direction, given by $H_B = -\Omega\sigma_z$, where $\Omega = \mu B$, with μ as the magnetic moment and B as the strength of the magnetic field. Consider an initial state of the form $|\psi(t)\rangle = \cos(\theta/2)|0\rangle + \sin(\theta/2)|1\rangle$. At a later time t the wave function will be $|\psi(0)\rangle = e^{i\Omega t/\hbar}\cos(\theta/2)|0\rangle + e^{-i\Omega t/\hbar}\sin(\theta/2)|1\rangle$. The period of the evolution is $\tau = \pi\hbar/\Omega$. By direct evaluation we can see that $|\psi(\tau)\rangle = -|\psi(0)\rangle$ and $\phi = \pi$. Thus, by solving the integral in Eq. (1.3.3) we get:

$$\beta = \pi(1 - \cos\theta). \tag{1.3.5}$$

A noteworthy property of this example is that the geometrical phase corresponds to half the angle enclosed by the loop on the Bloch sphere [17, 19]. This example is thus clarifying because this description in terms of the Bloch state helps us visualize what is happening geometrically. However, as we have stressed before, what is really important is the loop in the ray space $\mathcal{P}$, and not the path on the Bloch sphere itself, as this intuitive interpretation in terms of the Bloch sphere is a very particular property of our model and does not hold for all cyclic evolutions (just as the loop in the parameter space for the Berry phase is also just a particular case of a more general result).

We can now extend this result to the non-Abelian case, following the steps from [20]. Consider a n-dimensional subspace $V_n(t)$ of $\mathcal{H}$. We shall consider that evolution is cyclic so this subspace is the same for the endpoints of the dynamics, i.e. $V(0) = V(\tau)$. Now, consider a decomposition $H = V_n(t) \oplus V_m(t)$ of the Hilbert space into two subspace of dimension n and m, respectively. As we will see later, this type of division can be really natural. For example, in several applications, such as one we will choose later on, the computational space of the qubits is just of a subspace of a bigger Hilbert space, which may include auxiliary states into the implementation of a quantum gate. Another common application occurs when V_n is a degenerate eigenspace of H, such as it happens in the Wilczek-Zee phase [18].

Now, consider two orthonormal bases. First a basis $\{|\tilde{\psi}_a(t)\rangle, a = 1, ..., n\}$ of V_n which satisfies the cyclic condition $|\tilde{\psi}_a(\tau)\rangle = |\tilde{\psi}_a(0)\rangle$. And second, a basis $\{|\psi_a(t)\rangle, a = 1, ..., n\}$ which follows the SE:

$$i\hbar\frac{d}{dt}|\psi_a(t)\rangle = H|\psi_a(t)\rangle. \tag{1.3.6}$$

Both bases initially coincide $|\tilde{\psi}_a(0)\rangle = |\psi_a(0)\rangle$. These two bases will be related by a unitary matrix:

$$|\psi_a(t)\rangle = \sum_{b=1}^{n} U_{ba}(t)|\tilde{\psi}_b(t)\rangle. \tag{1.3.7}$$

By inserting the previous equation into Eq. (1.3.6) we obtain an explicit form for

the unitary, given by:

$$\boldsymbol{U}(t) = \mathcal{T} \exp\left(\int_0^t i(\boldsymbol{A} - \boldsymbol{K})dt\right). \tag{1.3.8}$$

Here $\mathcal{T}$ is the time ordering operator, $K_{ab} = (1/\hbar)\langle\tilde{\psi}_a| H |\tilde{\psi}_b\rangle$ corresponds to the dynamical part of evolution and $A_{ab} = i\langle\tilde{\psi}_a| d/dt |\tilde{\psi}_b\rangle$ corresponds to the geometrical part of the evolution. To see that, note that A_{ab} does *not* depend on H, but rather, only on the structure of the Hilbert space, i.e. it can be computed entirely from the basis $|\tilde{\psi}_a(t)\rangle$.

Investigating how A_{ab} transforms further clarifies its nature. By choosing a different basis $|\tilde{\psi}'\rangle = \boldsymbol{\Omega}|\tilde{\psi}\rangle$, where $\boldsymbol{\Omega}$ is a unitary, we can see that the two matrices transform as:

$$\boldsymbol{A} \to i\boldsymbol{\Omega}^\dagger\dot{\boldsymbol{\Omega}} + \boldsymbol{\Omega}^\dagger\boldsymbol{A}\boldsymbol{\Omega}, \quad \boldsymbol{K} \to \boldsymbol{\Omega}^\dagger\boldsymbol{K}\boldsymbol{\Omega}, \tag{1.3.9}$$

showing once again that $\boldsymbol{A}$ transforms as a vector potential and $i\langle\tilde{\psi}_a| d |\tilde{\psi}_b\rangle$ is a matrix-valued connection one-form. In this sense, we can say that $\boldsymbol{A}$ is a holonomy matrix for non-adiabatic evolutions [16].

This observation is important because it dictates the type of model and evolution we will be interested in. Namely, we are interested in loops for which the dynamical part $\boldsymbol{K}$ vanishes. This guarantees that evolution is purely geometric, for reasons presented before. In this case, from Eq. (1.3.8) we can write the unitary implemented by a loop C as

$$\boldsymbol{U}(C) = \mathcal{P} \exp\left(i \oint_C \mathcal{A}\right), \tag{1.3.10}$$

where $\mathcal{P}$ is the path-ordering operator. And finally, we are interested in the non-Abelian property of these phases, in other words, we should be able to obtain two different loops C and C' for which the corresponding unitaries (1.3.10) do not commute. As we will see in the next section, the Λ-type systems are a promising platform which satify both of these requirements.

2 Non-adiabatic quantum computing

2.1 The Λ-type system

The use of geometrical phases in quantum computing, while robust against certain types of noise and error [23], still suffers from decoherence and other open quantum system effects [24]. This calls for strategies that would circumvent this type of problem in some way [25]. Non-adiabatic holonomic quantum computing (NHQC) [16] has shown promise in performing this task [26]. The considerable speed-up in the operation time makes the system much more robust against decoherence. This configuration has been used before in a couple of different experimental systems, such as nitrogen-vacancy centers in diamond [27, 28] and superconducting qubits [29]. Other implementations which shorten the originally proposed protocol by employing single-loop holonomies were also investigated [30–33]. A generalization to discrete holonomies can be found in [34].

Here we will follow the original proposal for NHQC in the Λ-type-system from Ref. [16]. In this system, we couple two state $|0\rangle$ and $|1\rangle$ to an auxiliary excited state $|e\rangle$, while the two states $|0\rangle$ and $|1\rangle$, which span the qubit space, are uncoupled between themselves. Thus, the system acquires a Λ-like structure, depicted in Fig. 2.

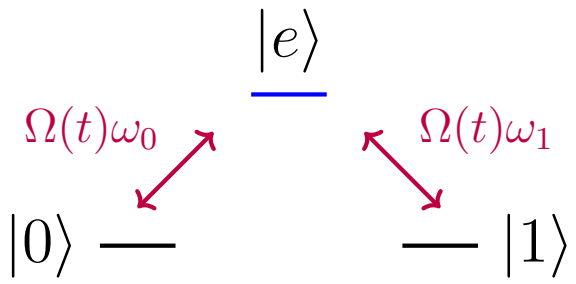

Figure 2: Basic setup for the Λ-type system.

The starting point is the Hamiltonian:

$$H(t) = H_0 + \boldsymbol{\mu} \cdot \boldsymbol{E}(t), \tag{2.1.1}$$

where $H_0 = -f_{e0} |0\rangle \langle 0| - f_{e1} |1\rangle \langle 1|$ is the bare Hamiltonian and

$$\boldsymbol{E}(t) = g_0(t) \cos(\nu_0 t)\boldsymbol{\epsilon}_0 + g_1(t) \cos(\nu_1 t)\boldsymbol{\epsilon}_1, \tag{2.1.2}$$

is the applied oscillating electric pulse. Here, $g_j(t)$ and ν_j (with $j = 0, 1$) are the pulse envelope and oscillation frequency, respectively. Additionally, $\boldsymbol{\mu}$ is the

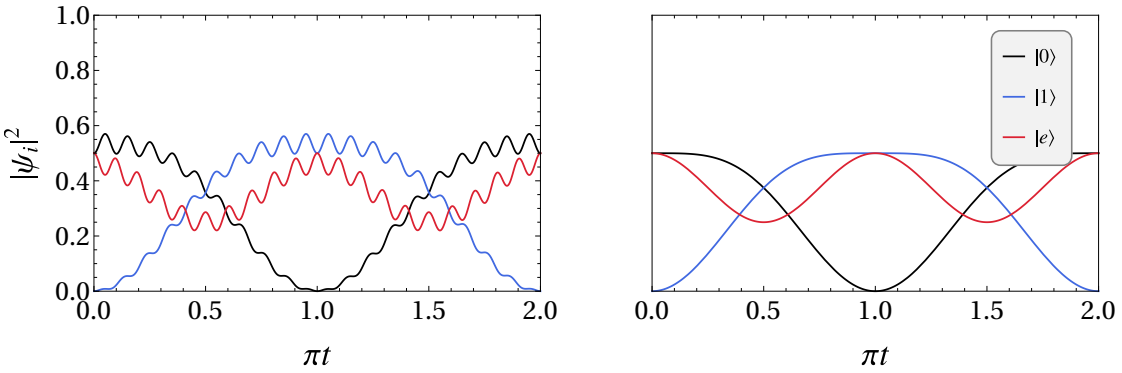

Figure 3: We compare the solutions of Eq. (2.1.4). We plot the populations (left) in the presence of counter-rotating terms, where $f_{e0} = f_{e1} = 10$ and $\Omega_0(t) = \Omega_1(t) = 1/\sqrt{2}$, and (right) in the RWA regime. In both cases we take the initial state to be $|\psi_0\rangle = (|0\rangle + |e\rangle)/\sqrt{2}$. As the frequencies f_{ei} increase, the smaller the ripples on the non-RWA solution get in comparison to overall period of the dynamics.

magnetic dipole moment operator and $\boldsymbol{\epsilon}$ is the polarization. We may then move on to the interaction picture Hamiltonian $H_I(t) = e^{-iH_0 t} H(t) e^{iH_0 t}$, obtaining:

$$\begin{aligned} H_I(t) = \Omega_0(t)(e^{-i(f_{e0}+\nu_0)t} + e^{-i(f_{e0}-\nu_0)t}) \left|e\right\rangle \left\langle 0\right| \\ + \Omega_1(t)(e^{-i(f_{e1}+\nu_1)t} + e^{-i(f_{e1}-\nu_1)t}) \left|e\right\rangle \left\langle 1\right| + \text{h.c.} \end{aligned} \tag{2.1.3}$$

In a final step, we tune the frequencies ν_j so they get resonant with the bare transition frequencies f_{ej}, i.e. $\nu_j = f_{ej}$. By doing so one finds:

$$H_I(t) = \Omega_0(t)(1 + e^{-2if_{e0}t}) \left|e\right\rangle \left\langle 0\right| + \Omega_1(t)(1 + e^{-2if_{e1}t}) \left|e\right\rangle \left\langle 1\right| + \text{h.c.} \tag{2.1.4}$$

where $\Omega_j = \langle e| \boldsymbol{\mu} \cdot \boldsymbol{\epsilon} |j\rangle \, g_j(t)/2$ are transition frequencies which depend only on the parameters of the applied field. Note how the bare Hamiltonian introduces counter-rotating terms of the type $(1 + e^{-2if_{ej}t})$. Throughout this work we will be interested in how to handle these terms and how they affect the quantum gates.

2.2 The role of the RWA

In this section we will be interested in how the counter-rotating terms previously mentioned affect the basic dynamics of the system and on how to perform the rotating-wave approximation (RWA) in a regime where these effects are negligible.

The argument here is that whenever f_{ei} is much bigger the other typical frequencies of the system, $e^{\pm 2if_{ej}t}$ become rapidly oscillating terms which average out to zero. This can be seen in more detail in Fig. 3. The counter-rotating terms introduces "ripples" in the solution. When we average out these terms, we get the

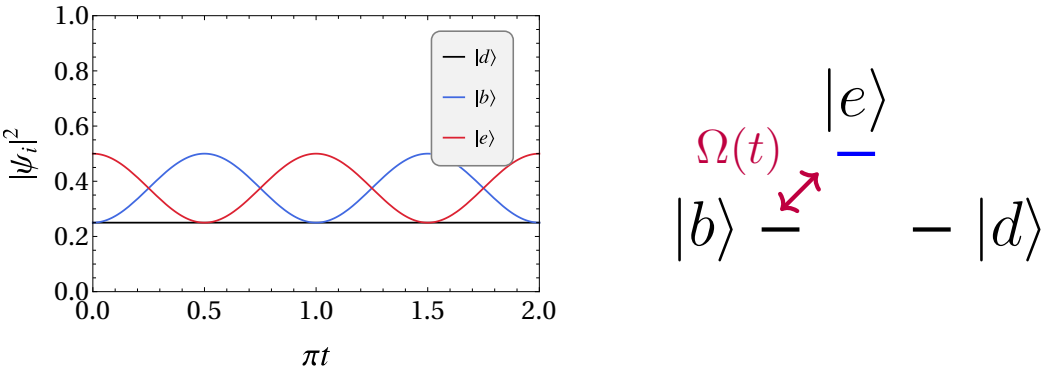

Figure 4: Evolution of the amplitudes of the state ψ_0 defined in Fig. (3) in terms of the bright and dark states (left). We also depict the Λ-type-system in this case (right).

RWA Hamiltonian

$$\mathrm{H}_I(t) = \Omega_0(t)\,|e\rangle\langle 0| + \Omega_1(t)\,|e\rangle\langle 1| + \mathrm{h.c}, \tag{2.2.1}$$

which has a periodic solution also seen on Fig. 3. Thus, it is possible to smooth out the dynamics of the system by increasing the energy gap of the bare states, approaching the RWA regime.

2.3 Bright and dark states

We can perform a very illustrative analysis on the Hamiltonian (2.2.1) in terms of its eigenstates. We define the dark state as $|d\rangle = -\omega_1\,|0\rangle + \omega_0\,|1\rangle$ and the bright state as $|b\rangle = \omega_0^*\,|0\rangle + \omega_1^*\,|1\rangle$. By doing so, we can rewrite Eq. (2.2.1) as:

$$\mathrm{H}_I(t) = \Omega(t)(|e\rangle\langle b| + |b\rangle\langle e|). \tag{2.3.1}$$

Here we introduce a frequency $\Omega(t)$ which let us rewrite the frequencies as $\Omega_0(t) = \omega_0\Omega(t)$ and $\Omega_1(t) = \omega_1\Omega(t)$, where we assume that $|\omega_0|^2 + |\omega_1|^2 = 1$. Thus, we can see that these states take theses names because with this change of basis we decouple the state $|d\rangle$ from evolution, and we effectively get a two-level system with oscillations between the bright state $|b\rangle$ and the auxiliary state $|e\rangle$. In Fig. (4) we depict the Rabi oscillations between these two states. Note how the amplitude of $|d\rangle$ remains unchanged throughout the evolution.

It is also meaningful to ask ourselves what happens when we perform this change of basis in the non-RWA case. When we do that, we get:

$$\begin{aligned} H_{bd}(t) = \Omega(t)(1 + |\omega_0|^2 e^{-2if_{e0}t} + |\omega_1|^2 e^{-2if_{e1}t})\,|e\rangle\langle b| \\ + \Omega(t)\omega_0\omega_1(e^{-2if_{e1}t} - e^{-2if_{e0}t})\,|e\rangle\langle d| + \mathrm{h.c.} \end{aligned} \tag{2.3.2}$$

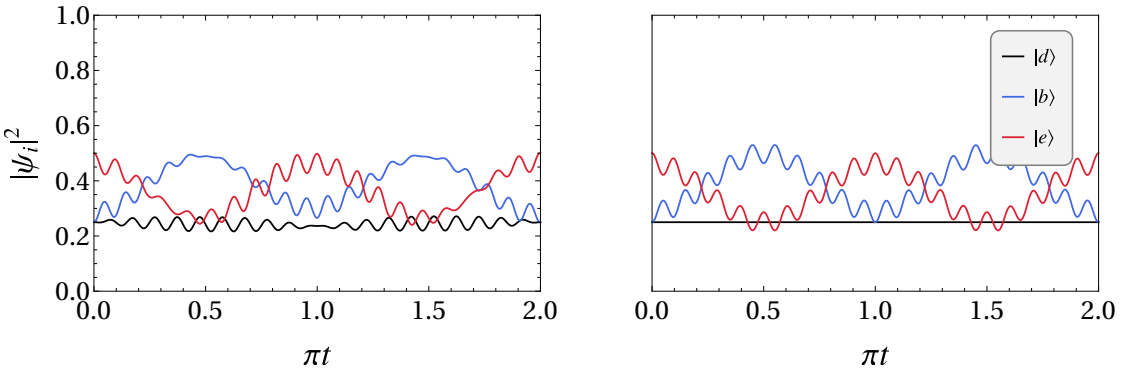

Figure 5: Dynamics of the amplitudes of the bright and dark states, acording to Eq. (2.3.2) with $f_{0e} = 10$ and $f_{1e} = 11$ (left) and Eq. (2.3.3) with $f_{0e} = f_{1e} = f = 10$ (right).

Notice that the counter-rotating terms, differently from RWA case, couple the dark state with the rest of the system. Thus, we lose this interesting property, which as we will see later on, will be fundamental for the single-qubit gates. However, the expression above assumes a particularly simple form when $f_{e1} = f_{e0} = f$, which is:

$$H_{bd}(t) = \Omega(t)(1 + e^{-2ift}) \, |e\rangle \langle b| + \text{h.c.} \tag{2.3.3}$$

When the two counter-rotating frequencies are the same this extra term cancels out and the dark state coupling vanishes. We show this effect concretely in Fig. 5. It may also be elucidating to examine what happens when we plot the trajectory of the state on the Bloch sphere. If we initialize the system in the state $|\psi_0\rangle = |b\rangle$ the amplitude of the dark state remains zero at all times, so it is possible to depict the evolution of the wave function on the Bloch sphere with poles $|b\rangle$ and $|e\rangle$. Results are shown in Fig. 6 for $\omega_0 = \omega_1 = 1/\sqrt{2}$.

It is interesting to note two things. As one would expect, the trajectory for the RWA is just a great circle around one of the axis, since the operator which appears in the Hamiltonian is just a Pauli matrix in the bright-dark basis. Meanwhile, the counter-rotating terms introduce a wobbling movement around the ideal path. One could think that even though the counter-rotating terms introduces oscillations the states still return to the initial points, but that, however, is not the case. In Fig. 6 we can also see that the wave function does not return to the initial state. Instead, what we observe is a new trajectory with a slight offset in comparison to the previous one. If we run the simulation for a long time it is possible to see in Fig. 6 (right) the cumulative effect of these slight deviations.

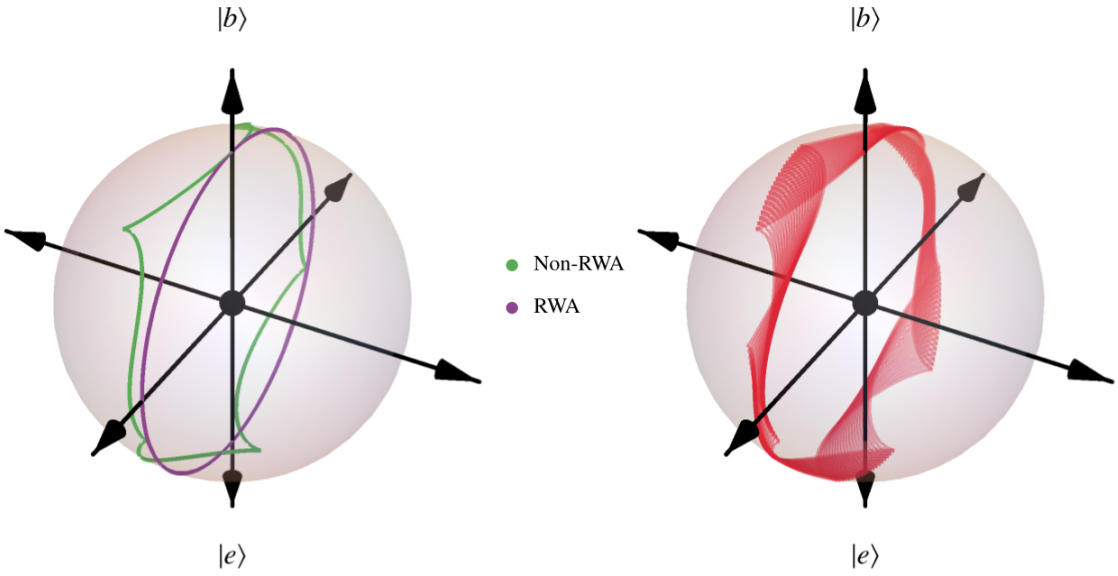

Figure 6: (Left) Trajectory of RWA and non-RWA evolution on the Bloch sphere for the state $|\psi_0\rangle = (|0\rangle + |1\rangle)/\sqrt{2}$. (Right) Trajectory on the Bloch sphere over a long time.

2.4 Implementing single-qubit gates

Here we will show how to use the geometrical properties of the Λ-type system in order to implement universal single-qubit gates. In our implementation we are interested in the qubit subspace $M(0) = \text{span}\{|0\rangle, |1\rangle\}$, while the state $|e\rangle$ plays the important auxiliary role. This space evolves into $M(t)$, which is spanned by:

$$|\psi_k(t)\rangle = \exp\left(-i\int_0^t H_f(t')dt'\right)|k\rangle = \mathcal{U}(t,0)\,|k\rangle\,, \tag{2.4.1}$$

where $k = 0, 1$ and $\mathcal{U}(t,0)$ is the time-evolution operator. It is also possible to get some insight into the dynamics by writing this in terms of the bright-dark basis. The unitary matrix becomes

$$\mathcal{U}_{bd}(t,0) = |d\rangle\langle d| + \cos(\Phi)(|b\rangle\langle b| + |e\rangle\langle e|) - i\sin(\Phi)(|e\rangle\langle b| + |b\rangle\langle e|) \tag{2.4.2}$$

which means that the bright and dark states evolve as [31]:

$$\begin{aligned} |\psi_d(\Phi)\rangle &= |d\rangle\,, \\ |\psi_b(\Phi)\rangle &= \cos(\Phi)\,|b\rangle - i\sin(\Phi)\,|e\rangle\,, \end{aligned} \tag{2.4.3}$$

where

$$\Phi = \int_0^t \Omega(t')dt' \tag{2.4.4}$$

is the area enclosed by the pulse. Geometrically, this evolution corresponds to a path in the Grassmanian $\mathcal{G}(3;2)$, i.e. the set of 2-dimensional subspaces of the 3-dimensional Hilbert space which defines the Λ system. In particular, when we have

$$\Phi = \Phi_C = \pi, \tag{2.4.5}$$

the trajectory corresponds to a full loop in the Grassmanian. Moreover, we can also see that the states evolve as

$$\begin{aligned} |\psi_d(\Phi_C)\rangle &= |d\rangle\,, \\ |\psi_b(\Phi_C)\rangle &= -\,|b\rangle\,, \\ |\psi_e(\Phi_C)\rangle &= -\,|e\rangle\,. \end{aligned} \tag{2.4.6}$$

The effect of this geometrical evolution whenever $\Phi = \pi$ is to implement a holonomy matrix Z_{bd} which acts by flipping the sign of $|b\rangle$ and $|e\rangle$ in the bright-dark basis. In other words:

$$\mathcal{U}_{bd}(C) = \begin{pmatrix} 1 & 0 & 0 \\ 0 & -1 & 0 \\ 0 & 0 & -1 \end{pmatrix}. \tag{2.4.7}$$

An explicit calculation shows that this matrix, in the computational basis, becomes, after properly projecting it into the qubit space:

$$U(C) = \mathcal{U}_{bd}(C)\mathbb{P} = \begin{pmatrix} \cos\theta & e^{-i\phi}\sin\theta \\ e^{i\phi}\sin\theta & -\cos\theta \end{pmatrix} = \boldsymbol{n}\cdot\boldsymbol{\sigma} \tag{2.4.8}$$

where $\boldsymbol{n} = (\sin\theta\cos\phi, \sin\theta\sin\phi, \cos\theta)$ and $\mathbb{P} = |0\rangle\langle 0| + |1\rangle\langle 1|$. Here, we have parametrized the frequencies ω_0 and ω_1 as $\omega_0 = \sin(\theta/2)e^{i\phi}$ and $\omega_1 = -\cos(\theta/2)$. Besides the convenient representation for the unitary, this also guarantees that $|\omega_0|^2 + |\omega_1|^2 = 1$. Thus, this process implements a π rotation around $\boldsymbol{n}$ on the Bloch sphere. This unitary, however, is not universal. By employing a second loop $C_{\boldsymbol{m}}$ we can implement the universal gate:

$$U(C) = U(C_{\boldsymbol{m}})U(C_{\boldsymbol{n}}) = \boldsymbol{n}\cdot\boldsymbol{m} - i\boldsymbol{\sigma}\cdot(\boldsymbol{n}\times\boldsymbol{m}). \tag{2.4.9}$$

This transformation has a clear geometrical meaning as well. The universal gate $U(C)$ above corresponds to a rotation in the plane spanned by $\mathbf{n}$ and $\mathbf{m}$ by an angle $2\cos^{-1}(\mathbf{n}\cdot\mathbf{m})$. Therefore, any single-qubit gate can be obtained by properly choosing the appropriate pulses, which will determine $\mathbf{n}$ and $\mathbf{m}$.

Under these considerations, we are going to choose a very convenient type of

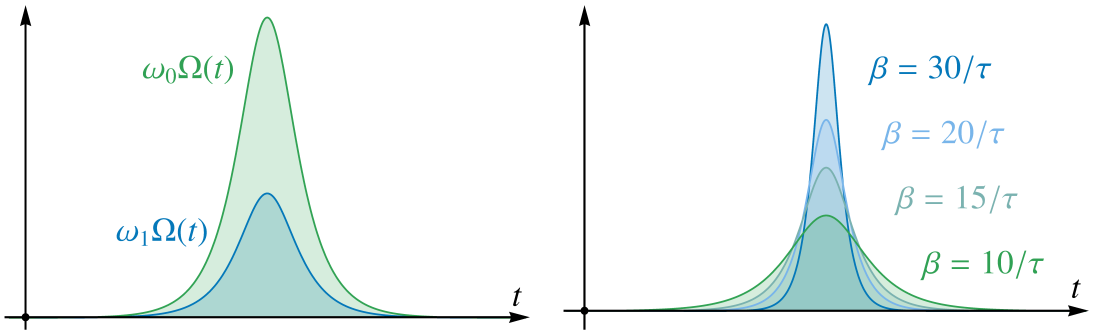

Figure 7: (a) A representation of the hyperbolic secant pulse from Eq. (2.4.10). (b) Representation of the pulse for different values of β. Note how $1/\beta$ can be seen as the length of the pulse. Here τ is an arbitrary time scale.

pulse, namely, pulses which have the shape of a hyperbolic secant:

$$\Omega(t) = \beta \sinh(\beta t). \tag{2.4.10}$$

This guarantees that the pulse is i) area-preserving for any β and that ii) Eq. (2.4.5) is also satisfied. This choice gives us freedom of using different pulse lengths just by changing the parameter β. As shown in Fig. 7(b), $1/\beta$ can be interpreted as the length of the pulse: pulses are sharper for large values of β and wider when β is small. Moreover, by appropriately choosing the angles θ and ϕ we can determine the vector $\mathbf{n}$ (and by choosing a different set of angles for the second pulse we determine $\mathbf{m}$).

As a practical example, we consider the Hadamard gate H and the T gate. For the Hadamard gate we need only a single pulse, choosing $\theta = \pi/4$ and $\phi = 0$. For the T-gate the protocol is slightly more complicated, since we need the two pulses. In this case, we can take $\theta_0 = \pi/2$ and $\phi_0 = \pi/2$ for the first pulse and $\theta_1 = 0$ and $\phi_1 = \pi/4$ for the second pulse.

The drawback of gates which require two loops, such as the T-gate, is that the exposure time to decoherence effects is longer. Protocols which implement non-adiabatic quantum gates for single-loops which can mitigate this effect can be found in [30] and [31].

2.5 Implementing two-qubit gates

In this section we once more follow the original proposal in [16], which also includes a protocol based on the Sørensen–Mølmer scheme [35] for implementing two-qubit gates (see also [14] for an adiabatic implementation and [36] for a generalization of the NHQC scheme for higher order gates). The setup for the two-qubit gate consists of two ions in the same three-level Λ configuration. The transition $0 \to e$ $(1 \to e)$

is driven by a laser with detuning $\nu \pm \delta$ ($\mp\nu \pm \delta$), where ν is the phonon frequency and δ is an additional detuning (see Fig. 8). Moreover, two extra conditions which the setup should satisfy are: the Lamb-Dicke criterion $\eta \ll 1$, where η is the Lamb-Dicke parameter, and $|\Omega_i(t)| < \nu$ in order to suppress the off-resonant couplings [35]. The Hamiltonian describing this interaction assumes the form:

$$H^{(2)} = \frac{\eta^2}{\delta}\left(|\Omega_0(t)|^2\sigma_0(\phi,t)\otimes\sigma_0(\phi,t) - |\Omega_1(t)|^2\sigma_1(-\phi,t)\otimes\sigma_1(-\phi,t)\right), \tag{2.5.1}$$

where

$$\begin{aligned}\sigma_0(\phi,t) &= e^{i\phi/4}(1+e^{-2if_{e0}t})\,|e\rangle\langle 0| + \text{h.c.},\\ \sigma_1(-\phi,t) &= e^{-i\phi/4}(1+e^{-2if_{e1}t})\,|e\rangle\langle 1| + \text{h.c.}\end{aligned} \tag{2.5.2}$$

After eliminating off-resonant couplings of the singly excited states $|0e\rangle$, $|e0\rangle$, $|1e\rangle$ and $|e1\rangle$ and performing the RWA the Hamiltonian reads:

$$H^{(2)}(t) = \sqrt{|\Omega_0(t)|^4 + |\Omega_1(t)|^4}\left(H_0^{(2)}(t) + H_1^{(2)}(t)\right), \tag{2.5.3}$$

with

$$H_0^{(2)}(t) = \sin\frac{\theta}{2}e^{i\phi/2}\,|ee\rangle\langle 00| - \cos\frac{\theta}{2}e^{-i\phi/2}\,|ee\rangle\langle 11| + \text{h.c.} \tag{2.5.4}$$

and

$$H_1^{(2)}(t) = \sin\frac{\theta}{2}\,|e0\rangle\langle 0e| - \cos\frac{\theta}{2}\,|e1\rangle\langle 1e| + \text{h.c.} \tag{2.5.5}$$

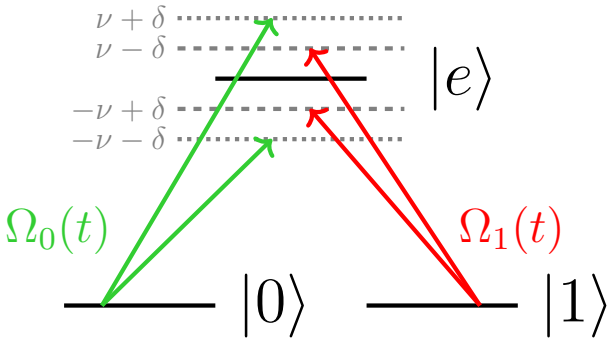

Figure 8: Setup for the ions in the two-qubit gate. The green (red) arrows and the dotted (dashed) lines correspond to the $\nu \pm \delta$ ($\nu \mp \delta$) detuning of the $0 \to e$ ($1 \to e$) transition. Both ions have the same configuration.

The criteria for two-qubit gate are analogous to what we have for the single qubit gates: the phase ϕ should be kept constant throughout the evolution, while

the frequencies satisfy $|\Omega_0(t)|^2/|\Omega_1(t)|^2 = \tan(\theta/2)$. Moreover, we should once again respect the criterion (2.4.5) for the pulse area:

$$\frac{\eta^2}{\delta}\int_0^\tau \sqrt{|\Omega_0(t)|^4+|\Omega_1(t)|^4}dt = \pi \tag{2.5.6}$$

However, one extra observation is in order; since $H_0^{(2)}(t)$ and $H_1^{(2)}(t)$ commute, it is possible to decompose the evolution of the total Hamiltonian (2.5.3) as

$$\exp\left(-i\int_0^\tau H^{(2)}(t)dt\right) = \exp\left(-i\pi H_0^{(2)}\right)\exp\left(-i\pi H_1^{(2)}\right). \tag{2.5.7}$$

The Hamiltonian $H_1^{(2)}(t)$ however acts trivially on the relevant computational subspace $\{|00\rangle, |01\rangle, |10\rangle, |11\rangle\}$ [16], making $H_0^{(2)}(t)$ the relevant term in the evolution. Due to this fact, $H^{(2)}(t)$ can be seen as a Λ-type-like Hamiltonian, and by analogy to the single qubit gate we get the corresponding unitary:

$$\begin{aligned} U^{(2)}(C_n) = {} & \cos\theta\,|00\rangle\langle 00| + e^{-i\phi}\sin\theta\,|00\rangle\langle 11| + e^{i\phi}\sin\theta\,|11\rangle\langle 00| \\ & - \cos\theta\,|11\rangle\langle 11| + |01\rangle\langle 10| + |10\rangle\langle 10|. \end{aligned} \tag{2.5.8}$$

This unitary acts just like a single qubit gate in the space $\{|00\rangle, |11\rangle\}$ and it leaves the components in the space $\{|01\rangle, |10\rangle\}$ invariant.

By choosing $\theta = 0$ we construct a CZ gate

$$U_{CZ}^{(2)} = |00\rangle\langle 00| + |01\rangle\langle 10| + |10\rangle\langle 10| - |11\rangle\langle 11|, \tag{2.5.9}$$

which is an entangling gate and can form a universal set together with other single-qubit gates [37].

Finally, if we take the counter-rotating terms into account, Eq. (2.5.10) and Eq. (2.5.11) become

$$H_0^{(2)}(t) = (1+e^{-2if_{e0}t})^2\sin\frac{\theta}{2}e^{i\phi/2}|ee\rangle\langle 00| - (1+e^{-2if_{e1}t})^2\cos\frac{\theta}{2}e^{-i\phi/2}|ee\rangle\langle 11| + \text{h.c.} \tag{2.5.10}$$

and

$$H_1^{(2)}(t) = 4\cos^2(f_{e0}t)\sin\frac{\theta}{2}|e0\rangle\langle 0e| - 4\cos^2(f_{e1}t)\cos\frac{\theta}{2}|e1\rangle\langle 1e| + \text{h.c.}, \tag{2.5.11}$$

respectively.

3 Open Quantum systems

In real world applications, decay and dissipative effects are phenomena which deeply constrain our implementation of functional quantum technologies. One of the major requirements for a good platform for quantum computing is the robustness against quantum noise and decoherence effects. In this sense, several approaches for formalizing the treatment of open quantum systems have emerged in the last decades [38–41]. In this section we will study some of these canonical formulations and how they can be applied to the Λ-type systems. Our objective is to show later on that the protocol is sufficiently robust against this type of effect.

3.1 Master Equations

One of most standard choices for describing open-quantum system effects is the Lindblad equation [42]. The Lindblad equation typically describes the interaction of a system, which is in contact with an external environment, undergoing some type of dissipative process, e.g. a qubit in contact with a thermal bath. Given a density matrix ρ which describes the state of the system, its dynamics is governed by

$$\frac{d\rho}{dt} = i[\rho, H] + \sum_k \gamma_k D_k(\rho), \tag{3.1.1}$$

where H is the Hamiltonian of the system and $D[\rho]$ is given by

$$D_k(\rho) = L_k \rho L_k^\dagger - \frac{1}{2}\{L_k^\dagger L_k, \rho\}. \tag{3.1.2}$$

The operators L_k are called jump operators and they describe different interactions between the system and the environment. The coefficients γ_k are simply coupling strengths associated with these interactions. We call Eq. (3.1.2) a *dissipator*. The matrix differential equation given by Eq. (3.1.1) is what we call the *Lindblad equation* and it describes the dynamics of the open system. The first term in this equation, which contains the commutator, is simply the von Neumann term and it describes the unitary evolution of the system. The dissipator on the other hand is responsible for taking dissipative and noisy effects into account.

3.2 Dissipative effect on the Λ-type system

In the Λ-type system, the excited state $|e\rangle$ is typically an unstable state which undergoes dissipation, while the computational states $|0\rangle$ and $|1\rangle$ can be regarded as stable ground states. Thus, a physical description of the model will look like Fig. 9. In our formulation we assume that the excited state decays to an auxiliary

ground state $|g\rangle$ which is *not* coupled to any other states through any type of unitary dynamics. This means that whenever the ground state is populated, these excitations are "lost" from the point of view of the computational subspace. This will result in a non-ideal mixed state at the end of the computation, which will decrease the overall fidelity of the gate. Our purpose is precisely to investigate how to mitigate this effect.

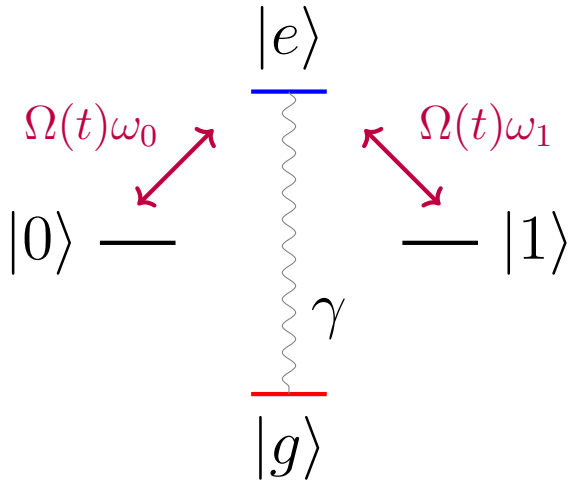

Figure 9: Basic setup for the Λ-type system when an open quantum system approach is considered. The excited state decays with a rate γ. There is no coupling or decay with the computational subspace itself. This means that dissipation effects only occur while the pulse is being applies and the excited state is populated.

We will model the decay with an amplitude-damping jump operator given by $L = |g\rangle\langle e|$. Under a purely dissipative evolution this term will push the excitations in $|e\rangle$ towards the ground state $|g\rangle$ (and, of course, this process will also damp the coherences of the system, together with the populations). Initially considering the RWA case, the dynamics of the system will then be given by

$$\frac{d\rho}{dt} = i[\rho, \mathrm{H}_I(t)] + \gamma D(|g\rangle\langle e|), \tag{3.2.1}$$

where $\mathrm{H}_I(t)$ is the RWA Hamiltonian in Eq. (2.2.1). Robustness against this type of noise has been shown in [16]. The takeaway message in this case was that the inverse pulse length should be much larger than the typical coupling strength γ, i.e. we should have $\beta \gg \gamma$. By increasing β the fidelity also monotonically increases, approaching unity. This is precisely one of the advantages of this non-adiabatic scheme: by removing constraints on the operation time one can use shorter pulses, diminishing the effects of decoherence.

By turning off the unitary part in Eq. (3.2.1) we can also understand how the dissipative part acts on the system as a sanity check. For a pure initial state of the type $|\psi\rangle = c_0 |0\rangle + c_1 |1\rangle + c_e |e\rangle$, the density matrix evolves as:

$$\rho(t) = \begin{pmatrix} |c_0|^2 & c_0 c_1^* & e^{-\gamma t/2} c_0 c_e^* & 0 \\ c_1 c_0^* & |c_1|^2 & e^{-\gamma t/2} c_1 c_e^* & 0 \\ e^{-\gamma t/2} c_e c_0^* & e^{-\gamma t/2} c_e c_1^* & e^{-\gamma t} |c_e|^2 & 0 \\ 0 & 0 & 0 & |c_e|^2 (1 - e^{-\gamma t}) \end{pmatrix}. \tag{3.2.2}$$

We can see that the process does not interfere with the computational subspace alone, but it dampens the population of the excited state and destroys the coherences. In the steady state limit $\gamma\tau \to \infty$, all the population from the excited state is transferred to the ground state. Hence, what happens when we turn off the unitary interaction is that the dissipative process occurs only during the pulse application, since there is no coupling between the computational subspace and the ground state. Thus, by shortening the pulse we also shorten the time during which the excited state is occupied and we minimize the errors due to dissipation. This is of course consistent with what we expected when choosing the jump operators to model the dissipation in this setup, so this result should not be seen as surprising.

We can now turn on the unitary part of interaction and try to quantify how well this protocol performs. For that, we will take the initial state $|\psi_0\rangle = |0\rangle$. Our gate of choice will be the Hadamard gate, whose implementation was discussed in Sec. 2.4. Ideally, the application of the Hadamard gate upon $|0\rangle$ should yield $|+\rangle = (|0\rangle + |1\rangle)/\sqrt{2}$.

The figure of merit for gate performance will be the fidelity, defined for two arbitrary mixed states ρ and σ as [43, 44]

$$F(\rho, \sigma) = \left(\mathrm{Tr} \sqrt{\sqrt{\rho} \sigma \sqrt{\rho}} \right)^2. \tag{3.2.3}$$

The fidelity essentially quantifies how similar two states are, being 0 for orthogonal states and 1 when both states are equal. Since we want to compare our output state with an expected result $|\psi\rangle$ which is always pure, the fidelity assumes a much simpler form. In this case, it will be

$$\mathcal{F} = F(\rho, |\psi\rangle \langle\psi|) = \langle\psi| \rho |\psi\rangle, \tag{3.2.4}$$

where $|\psi\rangle = U(C) |\psi_0\rangle$ is the ideal output upon the application of the ideal quantum gate $U(C)$ and ρ is the density matrix obtained by evolving the system under Eq. (3.2.1) for the whole duration of the pulse. We may also use the infidelity $1 - \mathcal{F}$ whenever it is convenient.

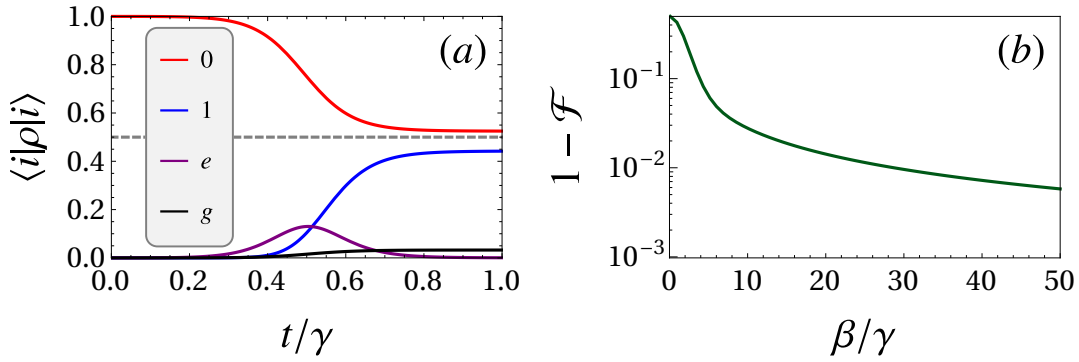

Figure 10: We plot (a) the populations of the density matrix for the implementation of the Hadamard gate and (b) the infidelity $1 - \mathcal{F}$ of the gate as a function of the pulse duration β. In both cases the input state is $|0\rangle$. The gray dashed line highlights the point $\langle i|\,\rho\,|i\rangle = 0.5$.

Basic results are shown in Fig. 10. On Fig. 10(a) we can see that the application of the pulse temporarily populates the excited state $|e\rangle$, transferring excitations from $|0\rangle$ to $|1\rangle$. Meanwhile, the ground state is also slightly populated due to these dissipative effects, and these excitations are "lost", in the sense that they are not recovered by the computational subspace later on in the evolution. And while we did not plot the coherences here, they are also affected by this dissipative process. For that reason the populations of $|0\rangle$ and $|1\rangle$ are not identical at the end of the protocol and we get a mixed state. We can quantify this effect by investigating how the duration β of the pulse changes the end result. In Fig. 10(b) we plot these results, showing the infidelity $1 - \mathcal{F}$ as a function of the pulse duration relative to the dissipation strength. We can see that it monotonically decreases as we increase β/γ.

4 Dropping the RWA

In the previous section we considered an implementation of the Λ-type system where the counter-rotating frequencies in Eq. (2.1.4) are rapidly oscillating compared to the typical timescales of the system, averaging out their effect to zero. This yields the RWA Hamiltonian (2.2.1), whose robustness under open quantum system effects we analyzed in Sec. 3.2. Our contribution here is to extend this treatment to finite frequencies, considering the Hamiltonian in Eq. (2.1.4), studying the interplay between the counter-rotating terms and the dissipative effects in the system.

An extension of the original proposal in [16] for the non-RWA case has been done previously in [45] for the dissipationless model. There, the authors show that the RWA starts to break down at very small operation times. The performance of the quantum gates is also analyzed for different pulse shapes and for typical experimental setups. An alternative approach to this problem is to look for strategies beyond the RWA, such as driven systems [46].

4.1 Sampling states on the Bloch Sphere

In order to quantify the performance of the Λ-type system implementation we calculate the fidelity given by Eq. (3.2.4) for input states uniformly distributed over the Bloch sphere. A common approach to this problem consists in sampling these points uniformly with respect to the Haar measure [26]. However, since computing the fidelity for a large number of points is computationally expensive, we turn instead to a simple algorithm called Fibonacci lattice (or nodes), which is reasonable approximation to evenly distribute a smaller number of points over the Bloch sphere. This approach is used to map points from a Fibonacci lattice in a square into a sphere through a cylindrical equal area projection [47]. This type of procedure is needed because a naive approach, where one uniformly samples the spherical angles, has a density of points strongly skewed towards the poles. This can been seen in Fig. 11, where we compare the uniform sampling with the so called Fibonacci nodes.

The procedure for a set of N points works as follows: i) uniformly distribute the z-coordinate of the points in the interval $[1, -1]$ into z_n, ii) distribute the azimuthal angle according to $\phi_n = 2\pi\varphi n$, where $\varphi = (1+\sqrt{5})/2$ is the golden ratio, and finally iii) take $x_n = \sqrt{1-z_n^2}\cos\phi_n$ and $y_n = \sqrt{1-z_n^2}\sin\phi_n$. The desire set of points will be given by the set of triples (x_n, y_n, z_n) for $n = 1, ..., N$. This procedure can, for instance, be used to uniformly generate points on the Bloch sphere.

One of the advantages of this method is that it is really simple to implement, and since the points are not distributed randomly, we can get a reasonably uniform

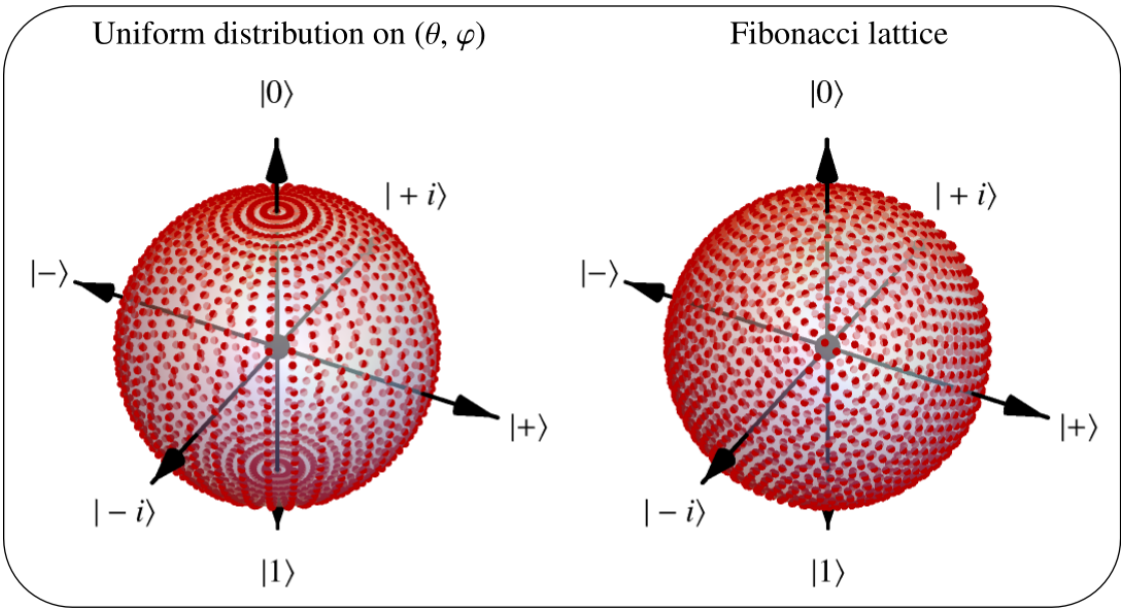

Figure 11: Distribution of points on the Bloch sphere. Compare the non-uniform distribution (left) with an approximately uniform distribution (right) given by Fibonacci nodes.

distribution even for a small number of points. Of course, if one is interested in methods which randomly distribute the points more canonical approaches are also available [48].

4.2 Combined effect of dissipation and counter-rotating terms

In this section we investigate the effect of the counter-rotating terms in the Λ-type system. For the single qubit gates we consider the Hamiltonian in Eq. (2.1.4) together with the dissipator for amplitude damping which appears in Eq. (3.2.1). The corresponding master equation

$$\frac{d\rho}{dt} = i[\rho, H_I] + \gamma D(|g\rangle \langle e|) \tag{4.2.1}$$

is then solved numerically for input states uniformly sampled on the Bloch sphere as described in Sec 4.1. The Λ-type system H_I is the unitary evolution, which implemented through a sequence of pulses, as described in Sec. 2.4, and it also contains the counter-rotating terms. The dissipator $D(|g\rangle \langle e|)$ describes the decay from the excited state to the ground state. The strength of this effect is encoded into the coupling parameter γ. The figure of merit used is the fidelity (3.2.4), which compares the expected (pure) output state and the density matrix we obtain at

the end of the simulation, resulting from the master equation.

As we have discussed before, the pulses $\Omega_0(t)$ and $\Omega_1(t)$ which implement the Hamiltonian (2.1.4) can be of arbitrary shape, provided they respect the pulse area $\Phi_C = \pi$, as shown in Eq. (2.4.5). Here we once again adopt the strategy of choosing hyperbolic sine pulses of the form (2.4.10). As previously discussed, the advantage of this choice is that β is a quantifier of how short the pulse is, while simultaneously preserving its area as π no matter the value of β.

Our main objective is to investigate the interplay between three components in this model: i) the pulse length β, ii) the counter-rotating frequencies $f_{e,i}$ and iii) the coupling parameter γ. Shorter pulses (larger β) make the dissipative effects negligible from the point of view of the system, this however also make the effect of the counter-rotating terms significant, and we observe a breakdown of the RWA if the frequencies f_{ei} are kept small. Conversely, using longer pulses in order to offset the counter-rotating frequencies also compromises the accuracy of the gate due to the long exposure time to dissipative effects. There is thus a "time-optimal" implementation of the single-qubit gates when one considers these effects jointly. Our numerical results agree with this intuitive idea.

We perform simulations for three different single-qubit gates. First for the X gate, which can be implemented through a single pair of pulses with $\omega_0 = e^{i\phi}\sin(\theta/2)$ and $\omega_1 = \cos(\theta/2)$, choosing $\theta = \pi/2$ and $\phi = 0$. Note that in this particular case both Rabi frequencies are the same. Secondly, we also perform simulations for the Hadamard gate, which can be implemented through a single pair of pulses with $\theta = \pi/4$ and $\phi = 0$. Finally, we also investigate the performance of the T gate, which can be implemented through a pair of pulses (note how this also explicitly showcases the need for a non-Abelian scheme), with $\theta_1 = \pi/2$ and $\phi_1 = 0$ for the first pair of pulses and $\theta_2 = \pi/2$ and $\phi_2 = \pi/4$ for the second one [16].

Basic results are shown in Fig. 12. We plot the fidelity as a function of the frequency f_i of the counter-rotating terms (in units of β), assuming $f_{e0} = f_{e1} = f_i$, for different values γ/β. The results are as one would expect: as the frequency of the counter-rotating term increases the fidelity converges to the fidelity of the RWA implementation, showing the validity of the approximation. Moreover, by decreasing γ/β the gate also performs better. All plots show this qualitative behavior.

One interesting point to note is that, for a same value of γ/β, the phase-shift gate in Fig. 12 (c) shows a slightly smaller fidelity when compared to the X and Hadamard gates in Fig. 12 (a) and Fig. 12 (b), respectively. The reason for that is the phase shift is implemented through two pairs of pulses, instead of a single one, as discussed before. This doubles the exposure time of the gate to dissipative effects, slightly diminishing its fidelity when compared to its single-pulse counterparts.

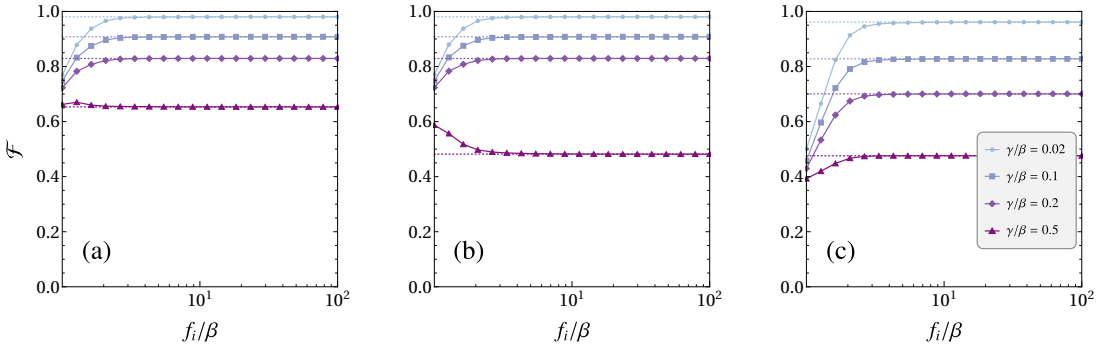

Figure 12: Fidelity as a function of the counter-rotating frequencies $f_{0e} = f_{1e} = f_i$ in units of β for (a) the X gate, (b) the Hadamard gate and (c) the T gate. The fidelity is calculated for 100 states uniformly sampled over the Bloch sphere. The dashed lines correspond to the fidelity in the RWA case. We can see that they are consistent with the numerical simulations for $f \gg \beta$.

These results let us conclude that in order to optimize the protocol one should have $f \gg \beta \gg \gamma$. This means that the counter-rotating frequencies should be much larger than the pulse length $1/\beta$. Fig. 13 illustrates this idea intuitively: by satisfying this condition the typical oscillations arising from the counter-rotating terms are much smaller than the dynamics generated by the pulses. At the same time the coupling γ should be much smaller than β. This is what it means to say that the pulse is short when compared to the dissipative effects, as $1/\beta$ is effectively setting the timescale for this comparison (of course, this choice is arbitrary and one could also compare the other two frequencies with γ instead).

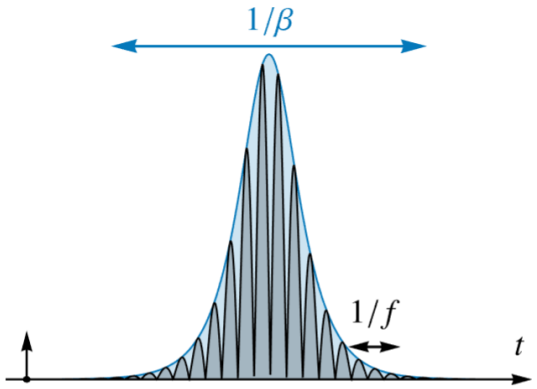

Figure 13: An illustration of the optimal regime. As one increases f the timescale of the pulse dominates and the RWA regime becomes valid, yielding a more accurate gate.

Meanwhile, in Fig. 14 we investigate the effect of different counter-rotating frequencies. For that we show a contour plot of the infidelity $1 - \mathcal{F}$ as a function

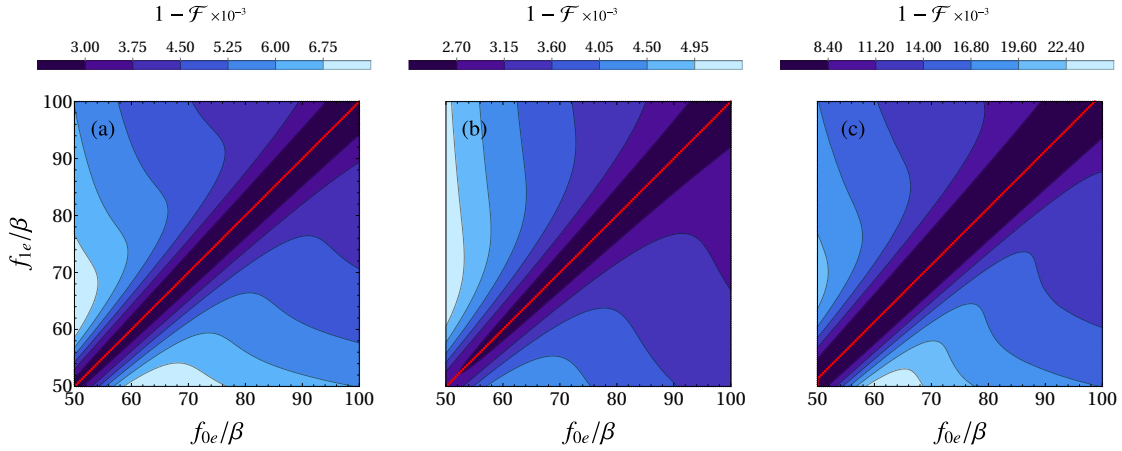

Figure 14: Average infidelity $1 - \mathcal{F}$ as a function of the counter-rotating frequencies f_{0e} and f_{0e} for $\gamma/\beta = 0.02$ for (a) the X gate, (b) the Hadamard gate and (c) the T gate. All other parameters and the input states are the same as in Fig. 12. The calculations were done for a grid of 150×150 frequencies f_{0e} and f_{1e}.

of both f_{0e} and f_{1e}. In red we plot the optimal value of f_{1e} for given f_{0e}. We can observe that for the X gate and the Hadamard gate, in Figs. 14 (a) and 14 (b), respectively, ideally one should always increase the two frequencies while taking them to be the same, i.e. $f_{0e} = f_{1e}$ for optimal gate performance. This is probably linked to the fact discussed in Sec. 2.3, where we showed in Eq. (2.3.3) how taking the counter-rotating frequencies to be the same *decouples* the dark state and the excited state in the dark-bright basis. So, in a sense, tuning $f_{e1} = f_{e0}$ further helps to reduce the effects of these counter-rotating terms. Meanwhile, we can also see that increasing one of the frequencies while keeping the other to be the same may decrease the fidelity of the gate.

We can see that in all of the three gates the optimal way to tune these frequencies is to increase them linearly with respect to each other. The optimal strategy for the X and the T gates is to keep them to be the same. For the T gate, on the other hand, while it is true that the two frequencies should be increased linearly in an optimal configuration, it seems that keeping f_{1e} slightly higher leads to a better performance.

Moreover, it is possible to note that Fig. 14 (a) displays a symmetric behaviour, while the other two do not. The reason for that is that the two pulses in the X gate are the same, this is not true for the Hadamard and the T gate. We can also clearly see that the infidelity of the T gate is higher when compared to the other gates. As we have discussed before, since the T gate requires two pairs of pulses the system will be much more susceptible to decoherence effects, due to the longer operation time.

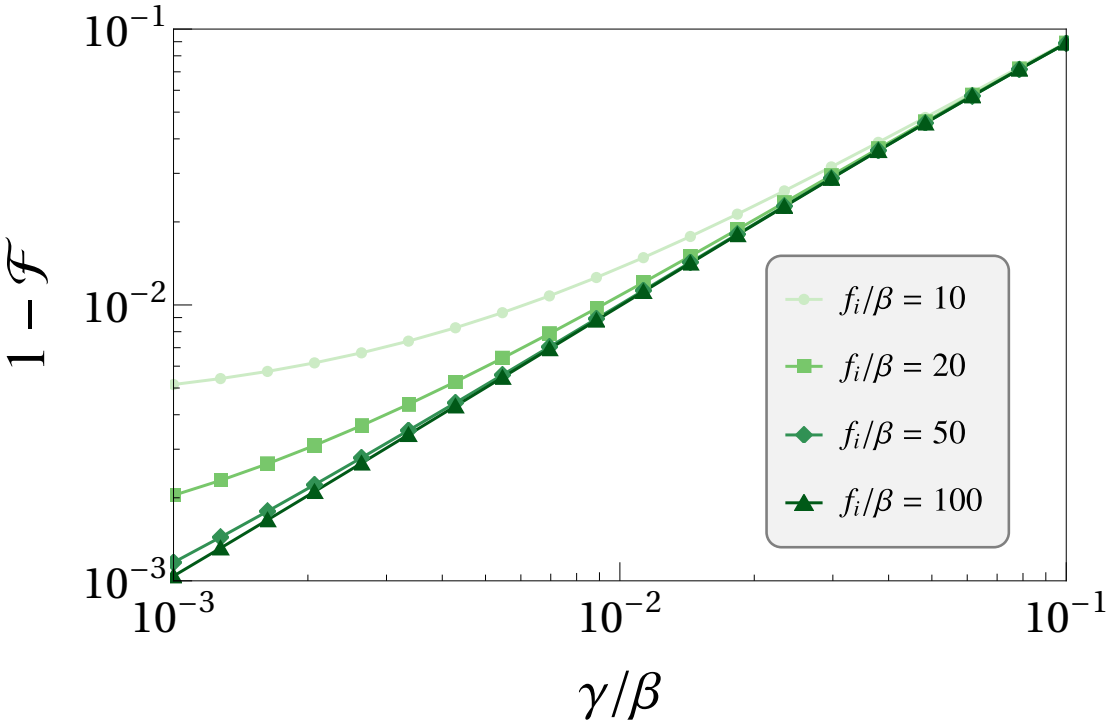

Figure 15: Average infidelity of the CZ gate for four different input states as a function of the (dimensionless) system-environment coupling parameter γ/β. Other parameters are as in the simulations for the single-qubit gates in Fig. 12.

Finally, we also investigate the fidelity of a two-qubit gate. We implement the CZ gate as described in Sec. 2.5. In Fig. 15 we plot the infidelity $1-\mathcal{F}$ of the gate averaged over four different input states, namely $|+\rangle|+\rangle$, $|+\rangle|-\rangle$, $|-\rangle|+\rangle$ and $|-\rangle|-\rangle$ with $|\pm\rangle = (|0\rangle \pm |1\rangle)/\sqrt{2}$.

These states were chosen because applying the CZ gate to these input states yield maximally entangled states. For instance, applying the CZ gate to $|+\rangle|+\rangle$ yields $CZ|+\rangle|+\rangle = (|0\rangle|+\rangle + |1\rangle|-\rangle)/\sqrt{2}$. If we apply a Hadamard gate H to the second qubit we get a Bell state, i.e. $(I\otimes H)CZ|+\rangle|+\rangle = \Phi_- = (|00\rangle - |11\rangle)/\sqrt{2}$. Our results show that the plots obtained for the two-qubit gate are qualitatively similar to what we have for single-qubit gates and that the gate is also robust against open quantum system effects under the appropriate conditions.

5 Conclusions

We have reviewed the basic framework for holonomic quantum computing, showing how non-adiabatic non-Abelian phases can be used to achieve high-speed quantum computing. Using a formalism for open quantum system we were also able to review some of the results for holonomic quantum gates and their robustness against decay.

Our main contribution was to further investigate the validity of the RWA in this model. In particular, we showed that there is a trade-off regarding the gate operation time; where shorter pulses are more robust against noise, but they however cause the RWA to fail. By analyzing the Λ-type system in the bright-dark basis we could also see that the counter-rotating terms in the Hamiltonian introduce a coupling between the dark and the excited states.

We obtained the regime and the parameters for which the gate operation is optimal. In particular, one should tune the pulse and the counter-rotating frequencies in a way that makes the pulse frequency much larger than the coupling between the system and the environment. On the other hand, the counter-rotating frequencies should be tuned in a way that their frequency is much larger then the inverse pulse length, which makes oscillations due to the counter-rotating terms negligible, recovering the RWA regime. Finally, we show the effect of asymmetric counter-rotating frequencies in the gate fidelity and their optimal configuration. We show that keeping both frequencies comparable yield optimal results.

The results obtained here could be extended to other generalizations of this basic setup, such as the single loop scheme [31] or the off-resonant scheme [30]. Strategies which do not rely on the RWA or a generalization to higher order gates could also be investigated.

References

[1] D. Deutsch and R. A. Jozsa, Proc. R. Soc. London. Ser. A **439**, 553 (1992).

[2] P. W. Shor, SIAM J. Comput. **26**, 1484 (1997).

[3] C. H. Bennett and G. Brassard, Theor. Comput. Sci. **560**, 7 (2014).

[4] D. P. DiVincenzo, Fortschritte der Phys. **48**, 771 (2000).

[5] P. W. Shor, Phys. Rev. A **52**, R2493 (1995).

[6] A. M. Steane, Phys. Rev. Lett. **77**, 793 (1996).

[7] J. Preskill, Proc. R. Soc. London. Ser. A **454**, 385 (1998).

[8] E. Joos and H. D. Zeh, Z. Phys. B **59**, 223 (1985).

[9] W. G. Unruh, Phys. Rev. A **51**, 992 (1995).

[10] A. Barenco, C. H. Bennett, R. Cleve, D. P. DiVincenzo, N. Margolus, P. Shor, T. Sleator, J. A. Smolin, and H. Weinfurter, Phys. Rev. A **52**, 3457 (1995).

[11] J. I. Cirac and P. Zoller, Phys. Rev. Lett. **74**, 4091 (1995).

[12] A. Kitaev, Ann. Phys. (N. Y.) **303**, 2 (2003).

[13] P. Zanardi and M. Rasetti, Phys. Lett. A **264**, 94 (1999).

[14] L.-M. Duan, J. I. Cirac, and P. Zoller, Science **292**, 1695 (2001).

[15] J. Zhang, T. H. Kyaw, S. Filipp, L.-C. Kwek, E. Sjöqvist, and D. Tong, (2021), arXiv:2110.03602 .

[16] E. Sjöqvist, D. M. Tong, L. Mauritz Andersson, B. Hessmo, M. Johansson, and K. Singh, New J. Phys. **14**, 103035 (2012).

[17] M. V. Berry, Proc. R. Soc. London. Ser. A **392**, 45 (1984).

[18] F. Wilczek and A. Zee, Phys. Rev. Lett. **52**, 2111 (1984).

[19] Y. Aharonov and J. Anandan, Phys. Rev. Lett. **58**, 1593 (1987).

[20] J. Anandan, Phys. Lett. A **133**, 171 (1988).

[21] J. J. Sakurai and J. Napolitano, *Modern Quantum Mechanics* (Cambridge University Press, 2020).

[22] S. M. Girvin and K. Yang, *Modern Condensed Matter Physics* (Cambridge University Press, 2019).

[23] L. Viotti, F. C. Lombardo, and P. I. Villar, (2021), arXiv:2110.14517 .

[24] P. Shen, T. Chen, and Z.-Y. Xue, Phys. Rev. Appl. **16**, 044004 (2021).

[25] J. Zhang, T. H. Kyaw, D. M. Tong, E. Sjöqvist, and L.-C. Kwek, Sci. Rep. **5**, 18414 (2016).

[26] M. Johansson, E. Sjöqvist, L. M. Andersson, M. Ericsson, B. Hessmo, K. Singh, and D. M. Tong, Phys. Rev. A **86**, 062322 (2012).

[27] C. Zu, W.-B. Wang, L. He, W.-G. Zhang, C.-Y. Dai, F. Wang, and L.-M. Duan, Nature **514**, 72 (2014).

[28] S. Arroyo-Camejo, A. Lazariev, S. W. Hell, and G. Balasubramanian, Nat. Commun. **5**, 4870 (2014).

[29] A. A. Abdumalikov Jr, J. M. Fink, K. Juliusson, M. Pechal, S. Berger, A. Wallraff, and S. Filipp, Nature **496**, 482 (2013).

[30] E. Sjöqvist, Phys. Lett. A **380**, 65 (2016).

[31] E. Herterich and E. Sjöqvist, Phys. Rev. A **94**, 052310 (2016).

[32] B. B. Zhou, P. C. Jerger, V. O. Shkolnikov, F. J. Heremans, G. Burkard, and D. D. Awschalom, Phys. Rev. Lett. **119**, 140503 (2017).

[33] Y. Xu, W. Cai, Y. Ma, X. Mu, L. Hu, T. Chen, H. Wang, Y. P. Song, Z.-Y. Xue, Z.-q. Yin, and L. Sun, Phys. Rev. Lett. **121**, 110501 (2018).

[34] C. J. G. Mommers and E. Sjöqvist, Phys. Rev. A **105**, 022402 (2022).

[35] A. Sørensen and K. Mølmer, Phys. Rev. Lett. **82**, 1971 (1999).

[36] P. Z. Zhao, G. F. Xu, and D. M. Tong, Phys. Rev. A **99**, 052309 (2019).

[37] M. J. Bremner, C. M. Dawson, J. L. Dodd, A. Gilchrist, A. W. Harrow, D. Mortimer, M. A. Nielsen, and T. J. Osborne, Phys. Rev. Lett. **89**, 247902 (2002).

[38] A. G. Redfield, Adv. Magn. Opt. Reson. **1**, 1 (1965).

[39] H.-P. Breuer and F. Petruccione, *The Theory of Open Quantum Systems* (Oxford University Press, 2007).

[40] J. Piilo, S. Maniscalco, K. Härkönen, and K.-A. Suominen, Phys. Rev. Lett. **100**, 180402 (2008).

[41] S. Scopa, G. T. Landi, A. Hammoumi, and D. Karevski, Phys. Rev. A **99**, 022105 (2019).

[42] G. Lindblad, Commun. Math. Phys. **48**, 119 (1976).

[43] A. Uhlmann, Reports Math. Phys. **9**, 273 (1976).

[44] R. Jozsa, J. Mod. Opt. **41**, 2315 (1994).

[45] J. Spiegelberg and E. Sjöqvist, Phys. Rev. A **88**, 054301 (2013).

[46] M. M. Gontijo and J. C. A. Barata, Phys. Scr. **95**, 055101 (2020).

[47] D. P. Hardin, T. J. Michaels, and E. B. Saff, Dolomites Res. Notes Approx. **9**, 16 (2016).

[48] M. E. Muller, Commun. ACM **2**, 19 (1959).